Large CO_2 seeps and hydrates field in the Indian Ocean (Mayotte Island)

Cécile Cathalot

Cecile.Cathalot@ifremer.fr

IFREMER https://orcid.org/0000-0002-0868-7201

Emmanuel Rinnert

IFREMER, Unité Géosciences Marines, Technopole La Pointe du Diable, 29280 Plouzané, France

Carla Scalabrin

IFREMER https://orcid.org/0000-0001-9276-980X

Olivia Fandino

IFREMER, UMR6538 Geo-Ocean

Thomas Giunta

Univ Brest

Hélène Ondreas

IFREMER, UMR6538 Geo-Ocean

Olivier Rouxel

IFREMER https://orcid.org/0000-0002-1431-222X

Christophe Rabouille

LSCE/IPSL, CEA-CNRS-UVSQ, UMR 8212

Jean-Pascal DUMOULIN

CNRS

Bruno Bombled

LSCE/IPSL, CEA-CNRS-UVSQ, UMR 8212

Marine Manoux

IFREMER, UMR6538 Geo-Ocean

Sharon Walker

NOAA/PMEL

Valérie Chavagnac

Université de Toulouse https://orcid.org/0000-0002-7535-6568

Andrea Rizzo

Università degli Studi di Milano-Bicocca, INGV

Morgan Tardivel

IFREMER, LDCM

Enora Prado
IFREMER, LDCM
Maria El Rawke
IFREMER, LDCM
Manon Mastin
IFREMER, UMR6538 Geo-Ocean
Jean-Pierre Donval
IFREMER, UMR6538 Geo-Ocean
Vivien Guyader
IFREMER, Unité Géosciences Marines, Technopole La Pointe du Diable, 29280 Plouzané, France
https://orcid.org/0000-0001-7296-1335
Gabrielle Page
IFREMER, BEEP
Marjolaine Matabos
Institut français de recherche pour l'exploitation de la mer https://orcid.org/0000-0003-1983-9896
Nathalie Feuillet
Institut de Physique du Globe de Paris (IPGP) https://orcid.org/0000-0001-6497-817X

Physical Sciences - Article

Keywords:

Posted Date: August 1st, 2024

DOI: https://doi.org/10.21203/rs.3.rs-4720763/v1

Additional Declarations: There is **NO** Competing Interest.

Abstract

About 80% of Earth volcanic activity occurs underwater, releasing deep carbon to submarine environments and impacting Earth's climate over geological timescales. The CO_2 emitted during submarine eruptions and/or hydrothermal degassing creates local ocean acidification, affecting the seawater carbonate equilibrium and oceanic ecosystems at large regional scales. Here, we report for the first time the existence of a major CO_2 hydrates field at the seafloor offshore Mayotte Island (Indian Ocean) associated with liquid CO_2 venting, following the submarine eruption that occurred in 2018. Using detailed acoustic surveys and *in situ* Raman spectroscopy, we reveal multiple hydrate mounds and seep zones distributed over an area of 0.06 km². We show that the gas seeps are mainly composed of CO_2, with minor contributions of CH_4 and H_2, with noble gas ratios and stable and radio-carbon isotopes clearly demonstrating their magmatic origin. Estimates of the CO_2 emitted over the entire area represent about 0.5% of the global magmatic carbon flux. Our discovery also suggests that CO_2 hydrates may potentially be stable at the seafloor at the right pressure-temperature conditions, bringing new prospects into CO_2 sequestration and decarbonization pathways in the ocean, in particular regarding kinetics of hydrates dissolution and environmental impacts.

Introduction

Volcanism is the main pathway to release carbon stored in the Earth's interior. In the preindustrial era, volcanic outgassing represented up to 90% Earth's surface carbon emission[1]. Current estimates suggest that most global volcanic outgassing occurs in submarine intraplate volcanic regions through diffuse emissions, the rest being distributed between mid-ocean ridges and subduction zones[2]. Although current anthropogenic fluxes overshadow volcanic ones, the long-term fluxes of carbon from solid Earth to the atmosphere have been dominated by volcanic sources over most of Earth's history with significant climatic impacts over geological timescales[3]. Massive and rapid volcanic CO_2 emissions to the atmosphere have led to severe global warming, ocean anoxia and acidification with lethal consequences for terrestrial and marine life[4].

Our understanding of the magnitude of CO_2 fluxes emitted from volcanic and magmatic active regions on Earth continues to evolve[5]. Contribution of submarine volcanic sources to the global budget, including direct and diffuse emissions might be largely underestimated due to lack of direct observation, poor fluxes quantification and remote and challenging site locations[6,7]. The eruption and creation of Fani Maoré volcano offshore Mayotte Island is, to date, the largest and deepest (3500 – 2700 m) deep-sea eruption to be studied both during and after the eruption[8]. As observed during most submarine volcanic eruptions, the Fani Maoré eruption released important quantities of magmatic volatiles[9,10] among which CO_2, H_2, and noble gases[11] along with metals and metalloids[11,12] with ambiguous impacts on adjacent and peripheral ecosystems in the deep ocean[11,13–15].

Very few occurrences of liquid CO_2 venting have been observed at the seafloor and, to our knowledge, there has not been any direct observation of CO_2-hydrates sitting on the seafloor in the deep ocean[16–18]. CO_2 hydrates formed upon contact between seawater and CO_2-rich fluid bubbles have been reported in the Okinawa Trough as small horn-shaped pipes (10 cm) quickly washed away[18], while most other observations have been inferred as embedded in sediment and/or associated with methane hydrates. While current industrial solutions for carbon dioxide sequestration via gas hydrates at the seafloor are being investigated[19,20], major questions remain regarding their short and long-term stability and potential impacts on surrounding seawater ecosystems, especially in case of CO_2 leakage[20]. Direct evidence in the field is critically needed to provide ground truthing about formation kinetics of CO_2 hydrates, efficiency of hydrate caps or films against CO_2 dissolution and resilience of impacted ecosystems[21].

Here we present the results of the GeoFLAMME sea expedition onboard RV Pourquoi Pas? offshore Mayotte Island (Comores Archipelago) following the Fani Maoré submarine eruption. Combining acoustic and water column data, sampling,video footage and *in situ* Raman spectroscopy, we provide evidence of a major submarine CO_2 hydrate field located in the Horseshoe area, 10 km east of Mayotte and 40 km west of the Fani Maoré volcanic edifice, associated with the release of mantle-derived liquid CO_2 likely driven by the eruption. We show that the generated CO_2 fluxes are equivalent to those from the most active volcanoes on Earth and result in significant local acidification, with impact on local benthic and pelagic ecosystems.

The Horseshoe edifice: a large liquid CO2 venting and hydrate field area

The Horseshoe edifice is a 4 km-wide collapsed volcanic cone. A major collapse resulted in the formation of a 2 km-wide depression at its center that opens to the north. Its crest is marked by a sharp and well-defined U-shaped limit: the Horseshoe's rim[22]. The Horseshoe area lies on the submarine flank of Mayotte in the depth range of 1200–1600 m, aligned along a west-northwest–east-southeast-trending volcanic ridge, with Fani Maoré at its easternmost tip[22]. The seafloor in the Horseshoe area is characterized by pumice mixed bioclastic-volcanoclastic content, including fresh phonolitic lava and bomb rims, confirming the volcanic origin and past activity of the edifice[23,24].

Since 2019, water column acoustic surveys using vessel hull multibeam echosounder were performed within the REVOSIMA monitoring program, allowing for the extensive mapping of the Horseshoe area, and the identification of vigorous acoustic plumes. Indeed, we discovered two active fluid emission sites in the Horseshoe area in May 2019, and by May 2021, that number had reached 15. These focused fluid flows cover an area of 0.063 km² over the ≈ 40 km² of the Horseshoe structure. They are mainly distributed over seven major zones, most around the Horseshoe rim, but also within the depression and at the eastern outside corner. (Fig. 1).

In spring 2021, the remotely operated vehicle (ROV) Victor 6000 revealed that each active site hosted a few to a hundred distinct fluid outlets (Table 1). Droplets rising from the seafloor were seen both with and without a milky skin. In addition, ROV images showed extensive presence of white milky patches and mounds either directly laying on the seafloor or inserted into crevices (Fig. 2). During an extensive survey in active site B0 (Fig. 1C), we counted at least 128 white mounds of different sizes and shapes, ranging from a few centimeters to 5 m high and up to ~ 1 m wide (SI video 1). Most grew in an almost columnar-like structure. The biggest mounds presented multiple liquid droplet streams rising from their bases and/or summits into the water column (Fig. 3G-J). On the Horseshoe rim structure, and along the ridge, steady stream and/or pulsing burst of droplets discharges were observed. Droplets escaped from open faults and cracks within the cliffs, and directly from holes in the gravel on the seafloor at the center depression of the Horseshoe area (Fig. 2). Filamentous microbial mats coated with oxidized iron compounds were observed in zone A, mostly between sites A1 and A2 (Fig. 2H). Flow rates were highly variable from one vent to another (Extended Data Table 1, Supplementary Table 1).

Table 1
Composition, isotopic signature and fluxes of CO_2 seeps in the Horseshoe area

A. Gas fluxes and composition in the Horseshoe area					
Site		**C4**	**C4**	**B0**	**B0**
Samples		GFL-PL778-09-PGZ01 #1	GFL-PL778-09-FLU1	GFL-PL779-10-PGZ03-#4	GFL-PL783-14-PGZ01-#12
Date of sampling		08/05/2021	08/05/2021	11/05/2021	21/05/2021
Type of sampler		PEGAZ	Gas tight syringe	PEGAZ	PEGAZ
Latitude		12°49,8827	12°49,8827	12°49,8275	12°49,8751
Longitude		45°23,0572	45°23,0572	45°22,7816	45°22,8430
Depth	m	1293	1293	1369	1357
Temperature recorded during sampling	°C	4–8	4–8	8.52	4.8–9.05
CO_2	%	98.89	98.04	94.70	98.93
CH_4	%	0.849	0.594	0.462	0.8
H_2	%	0.0012	0.0009	0.116	0.111
N_2	%	0.232	1.11	3.73	0.139
O_2	%	0.025	0.255	0.99	0.017
Rc/Ra	†	6.9	-	6.5	6.4
$\delta^{13}C$-CO_2	‰ vs PDB	-4.25	-	-4.5	-4.6
$\Delta^{14}C$-CO_2	‰	-995	-990	-998	-995

†R as $^3He/^4He$ in a sample; Ra as $^3He/^4He$ in air - see 31

B. Flux estimates			
Type of flow rates	**Measured CO_2 flow rates (avg ± std, n)**	**Number of fluid outlets in site B0**	**Estimated CO_2 fluxes * (avg ± std)**
	ml s^{-1}		tC y^{-1}
weak	5.7 ± 3.7 (3)	23	1.22 ± 1.01–10^4
medium	18.6 ± 7.7 (12)	119	2.79 ± 1.82 10^5
high	65.2 ± 32.3 (7)	17	1.40 ± 0.99 10^5
All types extrapolated over the entire Horseshoe Area			3.84 ± 2.59 10^5
** with density of liquid CO_2 of 0.98 kg m^{-3}*			
C. Comparison with other systems			
Volcanic systems	**Ref.**	**Estimated CO_2 fluxes (avg ± std)**	**Contribution of Horseshoe**
		GtC y^{-1}	%
Horseshoe area	this study	3.84 ± 2.59 10^{-4}	
Magmatic inputs			
MORB systems	2	0.016	2.4
All Magmatic C fluxes	2,44	0.072–0.079	0.49–0.53
Volcanic inputs			
El Hierro submarine volcano	45	2.19 10^{-4}	253.4
MOR systems	1,44	0.0264–0.097	0.2–0.8
All volcanic C fluxes	1	0.64	0.06

The liquid droplets were recovered and stored under pressure using the Pegaz device[25] for onshore analysis by gas chromatography[26]. They consist mainly of CO_2, 97.6 ± 2.0% v/v, with CH_4 as a minor secondary component, 0.7 ± 0.2% v/v. Similar to the liquid CO_2 previously observed at Champagne vent (NW Eifuku)[16], the droplets stuck to the ROV like clumps of grapes, and did not coalesce into larger droplets. The white patchy and mound structures consisted of a layer of milky-skin liquid CO_2 droplets. The film coating the droplets is likely CO_2 hydrates, which form from the interaction of CO_2 and water within the CO_2 hydrate stability zone conditions. The horseshoe area is well inside the stability conditions for both pure liquid CO_2 in pure water (387 m at 4°C) and pure CO_2 hydrates (200 m depth at 4°C). Presence of methane (or other chemicals) dissolved into the liquid CO_2 as well as the salinity may shift these melting points to slightly shallower depths. The mounds appear to be a more advanced stage of the patchy structures since they exhibit a hard core, which we hypothesize originates from the growth of the thin hydrate layer surrounding the liquid CO_2 droplet into bulk hydrate crystals.

Site B0 (Fig. 1) is one of the two seeping sites early detected in 2019 and the more extended in surface area. We therefore selected it for a detailed investigation of hydrates and CO_2 fountain morphology. CO_2 droplets presented different sizes and shapes: single droplets, droplets covered with a hydrate film, slender droplet formation or even tubular hydrates (Fig. 3, Supplementary Video 1), similar to what was observed at the JADE site in the Okinawa Trough[18] and varied according to flowrate, seep diameter and temperature, among other factors[27]. Ambient seawater temperature was ~ 4.3 °C compared to the fluid coming out of the seafloor of ~ 9 °C (Fig. 3E). All temperature measurements were made with the temperature probe in direct contact with the hydrate without drilling any holes. Temperature was not homogeneous along the hydrate surface at both mounds studied. Hydrate formation is an exothermic process, so active hydrate formation may locally increase the temperature of the hydrate surface.

We used *in situ* Raman spectroscopy to confirm the presence of CO_2 in a clathrate environment (not only under liquid form)[28,29] and to characterize the chemical composition of four mounds of different sizes chosen over a broad area to assess differences in the chemical composition of fluid emissions in the Horseshoe area. Chemical selectivity of gas hydrates is well known and their presence could modify the chemical composition of fluids reaching the water column. We measured temperature and Raman spectra at three different heights and inside a hole drilled in the mound using the ROV arms. The two spectra in Fig. 3E show the Raman signature of the Horseshoe seawater (shaded spectrum) and the white mounds (orange line). The two very strong vibrational bands C and D (Fermi resonance) indicate the presence of CO_2 in the white mounds. Corresponding to the OH bending mode of water, the vibrational band F is very intense in seawater but very weak in the solid sample. The difference in shape of the vibrational bands H and I (symmetric and asymmetric OH stretches) indicates that water molecules do not have the same structure in both samples, being compatible with the presence of water under a clathrate structure for the white mound sample. *In situ* Raman spectrum supports our visual observations: the white mounds are formed by liquid CO_2 in equilibrium with CO_2 hydrates and there is no evidence of methane or other gases entrapped in the gas hydrates, although presence of methane traces cannot be excluded given the sensitivity of the *in situ* Raman spectrometer. This is to our knowledge the first observation of natural CO_2 hydrates mounds on the seafloor.

Origin and ecological impact of the magmatic volatiles

Emitted fluids in the Horseshoe area generated small turbidity anomalies in the water column but high concentrations of ^3He, CH_4, CO_2 and H_2 and large decreases in Eh, pH and alkalinity compared to ambient seawater (Fig. 1, Extended Fig. 1, Supplementary Video 2). Fluid composition indicates that magmatic/hydrothermal gases are composed primarily of CO_2 and CH_4 with small contribution of H_2 (Table 1A), consistent with emissions at most other volcanoes[9,30–32] and in subaerial volcanic gasses from Mayotte Petite Terre[33]. The isotopic composition of CO_2 indicates a typical mantle[34] signature ($\delta^{13}C\text{-}CO_2$ = -3.7 ± 0.2‰, $\Delta^{14}C_{CO2}$ < -990‰). Since no molten lava is currently emitted at the seafloor in the Horseshoe area, H_2 likely originates from a magmatic/hydrothermal source[35] formed at depth along with CO_2 and dissolved within. Emitted fluids show very little variability with $^3He/^4He$ ratios (corrected for air contamination and expressed as Rc/Ra) of 6.62 ± 0.28 Ra, comparable to the values reported from gas emissions on Mayotte Petite Terre[33] and mantle xenoliths of Grande Comore[36]. This suggests a common magmatic source at depth likely aligned along an old fracture zone oriented N130 with potential secondary storage in gas saturated rocks located below the Horseshoe area[37].

Very few data are available for deep-sea habitats in the area, but this part of the Mozambique Channel is considered as a biodiversity hotspot[38]. To assess the impact of the CO_2 seeps on local and regional benthic ecosystems, we mapped the sessile megafaunal organisms present in the Horseshoe area during two ROV dives. Altogether, at least 23 morphotypes of cnidarians (class Anthozoa) were reported belonging to at least 5 orders (Extended Data Table 2). Identification from images in a newly explored area severely limits our ability to assess the actual biodiversity[39]. but our first observations are consistent with previous findings at shallower depths along the eastern slopes of Mayotte Island[39]. Anthozoans are abundant in and out of the Horseshoe area while sponges, belonging to Desmospongia and Hexactinellidae, are mainly found in the northern part and along the eastern ridge outside of the Horseshoe area (Fig. 4).

Most abundant morphotypes belonging to Octocorallia are identified as Alcyonacea gorgonian-like individuals which represented about almost half of all observed morphotypes (Extended Data Table 2). Few Actinaria are spotted close to the B and G active seeping zones (Fig. 4; Extended Data Fig. 2–4). Most individuals are found on the rim and cliffs of the Horseshoe structure, the base and centers being almost devoid of megafauna. We observe a significantly higher proportion of dead anthozoans close to the seep sites compared to “background” areas (Kruskal-Wallis chi-squared = 4.86, df = 1, p-value = 0.02749). The highest record of dead corals occurs in active seeping zones A and C, while zones B and G are almost devoid of sessile fauna. The little fauna visible corresponds to unidentified individuals covered by layers of sediment or microbial mats and hardly visible white fragments (supplementary material). Although individual species response may vary[40,41], the emitted fluids and resulting ~ 1 pH unit decrease observed in the water column within the Horseshoe area have indisputable impacts on the local deep-sea ecosystems, in particular for Scleratinian species. Deleterious effect of ocean acidification on cold-water corals but also adjacent planktonic, and even terrestrial, ecosystems have been demonstrated[4,42,43] and are therefore to be expected offshore Mayotte. Coral death related to a decrease in calcification rate can lead to major shifts in benthic communities[41], and eventually a loss in biodiversity. Mechanisms underlying changes in deep-sea ecosystem composition related to ocean acidification and submarine CO_2 release remain to be elucidated, and the Horseshoe area offers the ability to study potential remediation solutions.

CO2 budget and natural C sequestration laboratory

Quantitative estimates of the liquid CO_2 emissions on site B0 based on ROV video survey show that CO_2 fluxes represent 1.0 ± 0.10^{-4} GtC y^{-1}. Extrapolated to the entire Horseshoe area by hypothesizing that all the other 15 sites distributed over the seven major active zones display similar fluxes and seep densities, this leads to $3.84 \pm 2.59\ 10^{-4}$ GtC y^{-1} (Table 1B, Extended Data Table 3). Considering that the Horseshoe area is an active open window into local mantle C outputs[33], from a global perspective these fluxes amount about 2% of all Mid Ocean Ridges Basalts (MORB) and 0.5% of all magmatic fluxes[2,44]. While this may represent only 0.06 ± 0.04% of all volcanic fluxes[1] (Table 1C), several aspects need to be considered. 1) This is about twice the estimated fluxes emitted during the El Hierro eruption in 2011[45]. 2) The number of seep sites have been steadily increasing since 2019 and those fluxes therefore represent continuous ones rather than short-lived eruption-based emissions. 3) Consequently, we hypothesize that CO_2 hydrates have been forming ever since. These estimates do not take into account the standing reservoir stored as CO_2 hydrates, which alone at site B0 may represent 5 tC based on the 128 hydrates observed occurrences, with a median volume of $0.5 m^3$ and a density[46] of 1.1. Aside from its contribution to the regional carbon cycle and non-negligible C inputs, the Horseshoe area and its CO_2 gas hydrate field constitutes an unprecedented opportunity to study CO_2 sequestration pathways through gas hydrate formation. Such a large occurrence of naturally forming CO_2 hydrates may allow further studies regarding short- and long-term stability, kinetics of hydrates formation and dissolution in seawater[20]. In addition, monitoring liquid CO_2 vents may provide critical information regarding the environmental impacts of CO_2 leakage, in particular the ability of biological species to develop and adapt to low and variable pH conditions, and provide possible remediation solutions, or at least assess ecosystem vulnerability in natural conditions. High storage capacity and hydrate cap formation preventing CO_2 leaks make CO_2 hydrates attractive vehicles for deep ocean carbon sequestration[47,48]. However, observations of Horseshoe hydrates clearly indicate concomitant hydrate formation and CO_2 seeping, questioning the efficiency and safety of potential hydrate self-sealing process for preventing leakage as previously suggested in deep-sea sediment carbon sequestration studies[49,50]. A long-term seafloor observatory currently under construction in the Horseshoe area may constitute a first step to ground truth theoretical considerations regarding CO_2 hydrate decarbonization pathway. In addition, our discovery emphasizes the critical need to better understand ocean subseafloor processes, both in terms of fluid pathways, permeability and potential of CO_2 degassing, and in terms of relationships between tectonic/seismic and magmatic/thermal activity that might trigger and drive such CO_2 degassing events, locally affecting the ocean carbon cycle at multiple levels.

Methods

Water column acoustic data were collected with a dedicated acquisition protocol by vessel-hull mounted multibeam echosounders during the MAYOBS[51] cruises in 2019, 2020 and 2021 (Kongsberg™ EM122 12 kHz), and during the GEOFLAMME[52] cruise in 2021 (RESON™ 7150 24 kHz)., Data were post-processed with SonarScope (https://doi.org/10.17882/87777) and GLOBE (https://doi.org/10.17882/70460) software for the identification and location of the acoustic plumes[53].

A Sea-Bird Electronics™ CTD (SBE911plus) was used together with a rosette water sampler (SBE-32) equipped with 24 OTE 10L bottles for hydrographic measurements. For optical backscatter measurements a SeaPoint™ nephelometer were attached to the CTD probe. Upon CTD/rosette recovery, bottles were immediately sampled for gas, pH, silicates and total alkalinity analysis on board. pH was measured over 10ml samples using a Metrohm pH-meter, while total alkalinity measurements were performed over 10–30 ml water samples using Methrom titrimeter.

Gases analysis from hydrocast operations were performed onboard directly after sampling from unpoisoned samples. Hydrogen and Carbon dioxide concentrations were determined by headspace technique with HID detection[54] while Methane concentrations were determined by purge and trap technique coupled with GC-FID detection[55].

During the GEOFLAMME cruise, gas seeping from the vents (consisting mainly of liquid CO_2) was collected using the PEGAZ gas-bubble sampler[25]. In order to estimate seep fluid discharge and associated fluxes, 3D reconstruction of the seafloor based on ROV images, along with seep fluid counting and sampling were performed over zone B, specifically on site B0, one of the eldest and most vigorous sites. Immediately after recovery, the cylinder (50ml) of the PEGAZ sampler was positioned on a titanium cell equipped with a high pressure sensor and connected to a gas extractor for subsampling[26]. Once the vacuum has been achieved throughout the system, the Pegaz cylinder was first opened to the cell to evaluate the initial pressure. It was afterwards gradually opened to the gas extractor in order to expand, dry and subsample gases into vacuumed stainless-steel canisters of 50 to 1000 ml capacity equipped with gas-tight valves. Note that at ambient atmospheric pressure and temperature, liquid CO_2 decompresses quickly in the gas extractor and changes phase to a gas. The residual gas remaining in the extraction line was injected on board into an SRA Instruments ® micro-chromatograph for gas analysis[26]. Aliquots of extracted gases were also recovered in copper tubes for onshore analysis of helium and $\delta^{13}C_{CO2}$ isotopes at INGV[30,33]. To allow for a reasonable (and safe) CO_2 decompression in the extraction line, only one or two droplets of gases were collected with the PEGAZ sampler.

Radiocarbon analyzes were carried out on CO_2 droplets collected from the seeps around the hydrate field. The gas was collected, purified then converted to graphite[56] before being measured at the Artemis LMC14 AMS facility[57].

In situ Raman spectroscopy on hydrates mounds.

Visual recognition and identification of the white mounds was performed using the ROV video transects GFL-PL783-14 and GFL-PL785-16. Raman spectra were recorded using a "custom-made" spectrometer for *in situ* measurements named Ramses and mounted on the ROV[58,59] It is equipped with a Horiba Jobin Yvon axial spectrometer and can perform real-time Raman spectroscopy on liquids, gases, and solids at depths up to 4800 m. Housed in Titanium, it features a 600 gr/mm grating for a spectral resolution of 10 cm^{-1} and is equipped with two lasers (532 nm and 691 nm) for different sample types. It is coupled to an Andor DU440 CCD sensor.

Fluid flow rates estimates

Three ROV dives (GFL-ROV-PL776-07, GFL-ROV-PL778-09; GFL-ROV-PL785-16) were visually inspected to map, count and classify seep outlets of every active site in the entire Horseshoe area. A dedicated survey was performed in site B0 to quantify flow rates: a small funnel (530ml total volume) with volumetric graduation marks was used to measure flow rates on each event noted. The funnel was also deployed on site C1, D1, E0 and G0. Observed seeps were then classified into groups as a function of hydrate presence or absence and of liquid CO_2 flow rates low flow rate < 10 ml s^{-1}, medium flow rates between 10 and 40 ml s^{-1} and high flow rates > 40 ml s^{-1}. We calculated the number of seeps per category, average and standard deviation of the flow rate for each category. Density of seeps on site B0 was then calculated for each flow rate category and extrapolated over the entire Horseshoe area by assuming the same density repartition at all seeping sites than in site B0. Error estimate was set to 50% to account for site disparities. All annotated events and associated description and flux information are provided as supplementary material.

Megafauna mapping

Recognition and identification of megafauna was performed using the ROV videos acquired during GFL-PL07, GFL-PL16, and transects dedicated to the 3D reconstruction of site B. The Victor6000 has multiple cameras but because video acquisition was not set up for habitat mapping, the downward-looking camera could not be exploited properly. For this study we thus used the main ROV camera, and both the downward-looking and main cameras for site B. Images were analyzed using the ADELIE video annotation software using 3 criteria "sessile fauna category" (including dead Anthozoa), "organisms' density" and "substrata type". Because of the uncertainty in the identification of gorgonian- and coral-like morphotypes, these observations were grouped under the 'undetermined Anthozoa' modality (Extended Data Table 2). The definition of dead Anthozoa was based on the absence of color but also on the presence of living organisms around. For example, white corals observed among coloured corals or gorgonians were not considered as dead. Conversely, isolated colourless corals surrounded by broken sessile organisms covered by bacterial mats were annotated as 'dead'. During the annotation process, associated metadata (timecode, image name, geographical coordinates) were recorded with ADELIE software and compilation was performed on ArcGIS software. The opportunistic nature of this dataset did not allow for the acquisition of quantitative data and each faunal record was thus processed as one observation. To assess the impact of liquid CO_2 on faunal distribution, the mean proportion of each taxa, and 'dead' vs living corals, between active sites and background areas was compared using a Kruskall-Wallis test.

Declarations

Competing interests

The authors declare no competing interests

Author contributions

C. Cathalot, E. Rinnert, C. Scalabrin, O. Fandino, N. Feuillet, designed the work, lead the acquisition, analysis and interpretation of all data along with drafting the ms. H. Ondreas, acquired and interpreted CO_2 fluxes data. T.Giunta, O.Rouxel, M. Mastin., V. Chavagnac, A. L. Rizzo, J.P.Donval, V. Guyader, M. Manoux acquired, analyzed and interpreted chemical and isotopic fluid data. C.Rabouille, J.P. Dumoulin., B.Bombled acquired and interpreted ^{14}C data. S. Walker provided the MapR material and data interpretation. M. Tardivel, E. Prado, M. El Rawke acquired and interpreted *in situ* RAMAN data. G. Page and M. Matabos analyzed and interpreted all biological data. All authors contributed significantly to the ms and approved the submitted version.

Acknowledgements

We thank all the participants from the GEOFLAMME and MAYOBS sea expeditions, for their amazing work and support. We also thank the captains and crew members from R/V Pourquoi Pas?, along with the AUV and ROV Victor 6000 team (GENAVIR) crew members. We thank Delphine Pierre and Anne-Sophie Alix for their help in generating the Horseshoe map. This research was supported by the Mayotte volcanological and seismological monitoring network (REVOSIMA, doi: 10.18715/MAYOTTE.REVOSIMA), by the French Oceanographic Fleet, by TotalEnergies (TOTAL ENERGIES FR000063751 //876 IFREMER 20/1001730) and by ISblue project, Interdisciplinary graduate school for the blue planet (ANR-17-EURE-0015) and co-funded by a grant from the French government under the program "Investissements d'Avenir" embedded in France 2030. We are finally grateful to Mariano Tantillo and Igor Oliveri, who carried out helium and carbon isotopic analyses at INGV Palermo laboratories.

References

1. Burton, M., Sawyer, G. & Granieri, D. Deep Carbon Emissions from Volcanoes. Reviews in Mineralogy and Geochemistry 75, 323–354, doi:10.2138/rmg.2013.75.11 (2013).

2. Plank, T. & Manning, C. E. Subducting carbon. Nature 574, 343–352, doi:10.1038/s41586-019-1643-z (2019).
3. Tolstoy, M. Mid-ocean ridge eruptions as a climate valve. Geophysical Research Letters 42, 1346–1351, doi:10.1002/2014gl063015 (2015).
4. Cui, Y., Li, M., van Soelen, E. E., Peterse, F. & Kürschner, W. M. Massive and rapid predominantly volcanic CO < sub > 2</sub > emission during the end-Permian mass extinction. *Proceedings of the National Academy of Sciences* 118, e2014701118, doi:doi:10.1073/pnas.2014701118 (2021).
5. Lizarralde, D., Soule, S. A., Seewald, J. S. & Proskurowski, G. Carbon release by off-axis magmatism in a young sedimented spreading centre. Nature Geoscience 4, 50–54, doi:10.1038/ngeo1006 (2011).
6. Werner, C. *et al.* in *Deep Carbon: Past to Present* (eds Beth N. Orcutt, Isabelle Daniel, & Rajdeep Dasgupta) 188–236 (Cambridge University Press, 2019).
7. Orcutt, B. N., Daniel, I., Dasgupta, R., Crist, D. T. & Edmonds, M. in *Deep Carbon: Past to Present* (eds Beth N. Orcutt, Isabelle Daniel, & Rajdeep Dasgupta) 1–3 (Cambridge University Press, 2019).
8. Feuillet, N. *et al.* Birth of a large volcanic edifice offshore Mayotte via lithosphere-scale dyke intrusion. Nature Geoscience 14, 787–795, doi:10.1038/s41561-021-00809-x (2021).
9. Resing, J. A. *et al.* Active submarine eruption of boninite in the northeastern Lau Basin. Nature Geoscience 4, 799–806, doi:10.1038/ngeo1275 (2011).
10. Stucker, V. K., de Ronde, C. E. J., Laurence, K. J. & Phillips, A. M. Rare Time Series of Hydrothermal Fluids for a Submarine Volcano: 14 Years of Vent Fluid Compositions for Brothers Volcano, Kermadec Arc New Zealand. Economic Geology, doi:10.5382/econgeo.4922 (2022).
11. Mastin, M. *et al.* Strong geochemical anomalies following active submarine eruption offshore Mayotte. Chemical Geology 640, 121739, doi:https://doi.org/10.1016/j.chemgeo.2023.121739 (2023).
12. Rubin, K. Degassing of metals and metalloids from erupting seamount and mid-ocean ridge volcanoes: Observations and predictions. Geochim. Cosmochim. Acta 61, 3525–3542, doi:https://doi.org/10.1016/S0016-7037(97)00179-8 (1997).
13. Gómez-Letona, M., Arístegui, J., Ramos, A. G., Montero, M. F. & Coca, J. Lack of impact of the El Hierro (Canary Islands) submarine volcanic eruption on the local phytoplankton community. Scientific Reports 8, 4667, doi:10.1038/s41598-018-22967-6 (2018).
14. Mittal, T. & Delbridge, B. Detection of the 2012 Havre submarine eruption plume using Argo floats and its implications for ocean dynamics. Earth and Planetary Science Letters 511, 105–116, doi:https://doi.org/10.1016/j.epsl.2019.01.035 (2019).
15. Santana-Casiano, J. M. *et al.* The natural ocean acidification and fertilization event caused by the submarine eruption of El Hierro. Scientific Reports 3, 1140, doi:10.1038/srep01140 (2013).
16. Lupton, J. *et al.* Submarine venting of liquid carbon dioxide on a Mariana Arc volcano. Geochemistry, Geophysics, Geosystems 7, Q08007, doi:10.1029/2005GC001152 (2006).

17. Lupton, J. *et al.* Venting of a separate CO2-rich gas phase from submarine arc volcanoes: Examples from the Mariana and Tonga-Kermadec arcs. Journal of Geophysical Research: Solid Earth 113, B08S12, doi:10.1029/2007JB005467 (2008).
18. Sakai, H. *et al.* Venting of Carbon Dioxide-Rich Fluid and Hydrate Formation in Mid-Okinawa Trough Backarc Basin. Science 248, 1093–1096 (1990).
19. Park, Y. *et al.* Sequestering carbon dioxide into complex structures of naturally occurring gas hydrates. *Proceedings of the National Academy of Sciences* 103, 12690–12694, doi:doi:10.1073/pnas.0602251103 (2006).
20. Zheng, J., Chong, Z. R., Qureshi, M. F. & Linga, P. Carbon Dioxide Sequestration via Gas Hydrates: A Potential Pathway toward Decarbonization. Energy & Fuels 34, 10529–10546, doi:10.1021/acs.energyfuels.0c02309 (2020).
21. Shindo, Y., Lund, P. C., Fujioka, Y. & Komiyama, H. Kinetics of formation of CO2 hydrate. Energy Conversion and Management 34, 1073–1079, doi:https://doi.org/10.1016/0196-8904(93)90055-F (1993).
22. Puzenat, V. *et al.* Volcano-tectonic structures of Mayotte's upper submarine slope: insights from high-resolution bathymetry and in-situ imagery from a deep-towed camera. *C. R. Geosci.* Online first (2022), 1–24, doi:10.5802/crgeos.175 (2022).
23. Thivet, S. *et al.* Volatiles of the active Mayotte volcanic chain: STA & EGA-MS analysis of volcanic products. Chemical Geology 618, 121297, doi:https://doi.org/10.1016/j.chemgeo.2022.121297 (2023).
24. Paquet, F. *et al.* in *ASF 2022 - XVIIIème Congrès Français de Sédimentologie* (Brest, France, 2022).
25. Ruffine, L. *et al.* Gas Seepage along the Edge of the Aquitaine Shelf (France): Origin and Local Fluxes. *Geofluids* 2017, 4240818, doi:10.1155/2017/4240818 (2017).
26. Charlou, J. L. *et al.* Physical and chemical characterization of gas hydrates and associated methane plumes in the Congo–Angola Basin. Chemical Geology 205, 405–425, doi:https://doi.org/10.1016/j.chemgeo.2003.12.033 (2004).
27. Hirai, S. & Sanda, H. Injection and boiling of liquid CO2 with a hydrate coating. Energy 30, 2275–2283, doi:https://doi.org/10.1016/j.energy.2003.10.020 (2005).
28. Li, L. *et al.* In Situ Raman Spectral Characteristics of Carbon Dioxide in a Deep-Sea Simulator of Extreme Environments Reaching 300 °C and 30 MPa. Applied Spectroscopy 72, 48–59, doi:10.1177/0003702817722820 (2018).
29. Zhang, X. *et al.* In Situ Raman Detection of Gas Hydrates Exposed on the Seafloor of the South China Sea. Geochemistry, Geophysics, Geosystems 18, 3700–3713, doi:https://doi.org/10.1002/2017GC006987 (2017).
30. Rizzo, A. L. *et al.* Geochemistry of CO2-Rich Gases Venting From Submarine Volcanism: The Case of Kolumbo (Hellenic Volcanic Arc, Greece). Frontiers in Earth Science 7, doi:10.3389/feart.2019.00060 (2019).

31. Resing, J. A. *et al.* Chemistry of hydrothermal plumes above submarine volcanoes of the Mariana Arc. Geochemistry, Geophysics, Geosystems 10, doi:10.1029/2008gc002141 (2009).
32. Baumberger, T. *et al.* Dissolved Gas and Metal Composition of Hydrothermal Plumes From a 2008 Submarine Eruption on the Northeast Lau Spreading Center. Frontiers in Marine Science 7, doi:10.3389/fmars.2020.00171 (2020).
33. Liuzzo, M. *et al.* Gas Geochemistry at Grande Comore and Mayotte Volcanic Islands (Comoros Archipelago), Indian Ocean. Geochemistry, Geophysics, Geosystems 22, e2021GC009870, doi:https://doi.org/10.1029/2021GC009870 (2021).
34. Mason, E., Edmonds, M. & Turchyn, A. V. Remobilization of crustal carbon may dominate volcanic arc emissions. Science 357, 290–294, doi:doi:10.1126/science.aan5049 (2017).
35. Worman, S. L., Pratson, L. F., Karson, J. A. & Schlesinger, W. H. Abiotic hydrogen (H < sub > 2) sources and sinks near the Mid-Ocean Ridge (MOR) with implications for the subseafloor biosphere. *Proceedings of the National Academy of Sciences* 117, 13283–13293, doi:doi:10.1073/pnas.2002619117 (2020).
36. Bordenca, C. V. *et al.* Geochemical evidence for a lithospheric origin of the Comoros Archipelago (Indian Ocean) as revealed by ultramafic mantle xenoliths from La Grille volcano. Lithos 462–463, 107406, doi:https://doi.org/10.1016/j.lithos.2023.107406 (2023).
37. Foix, O. *et al.* Offshore Mayotte volcanic plumbing revealed by local passive tomography. Journal of Volcanology and Geothermal Research 420, 107395, doi:https://doi.org/10.1016/j.jvolgeores.2021.107395 (2021).
38. Obura, D. The Diversity and Biogeography of Western Indian Ocean Reef-Building Corals. PLOS ONE 7, e45013, doi:10.1371/journal.pone.0045013 (2012).
39. Hanafi-Portier, M. *et al.* When Imagery and Physical Sampling Work Together: Toward an Integrative Methodology of Deep-Sea Image-Based Megafauna Identification. Frontiers in Marine Science 8, doi:10.3389/fmars.2021.749078 (2021).
40. Form, A. U. & Riebesell, U. Acclimation to ocean acidification during long-term CO2 exposure in the cold-water coral Lophelia pertusa. Global Change Biology 18, 843–853, doi:10.1111/j.1365-2486.2011.02583.x (2012).
41. Comeau, S. *et al.* pH variability at volcanic CO2 seeps regulates coral calcifying fluid chemistry. Global Change Biology 28, 2751–2763, doi:https://doi.org/10.1111/gcb.16093 (2022).
42. Maier, C., Hegeman, J., Weinbauer, M. G. & Gattuso, J. P. Calcification of the cold-water coral Lophelia pertusa under ambient and reduced pH. Biogeosciences 6, 1671–1680 (2009).
43. Fraile-Nuez, E. *et al.* The submarine volcano eruption at the island of El Hierro: physical-chemical perturbation and biological response. Scientific reports 2, 486–486, doi:10.1038/srep00486 (2012).
44. Marty, B. & Tolstikhin, I. N. CO2 fluxes from mid-ocean ridges, arcs and plumes. Chemical Geology 145, 233–248, doi:https://doi.org/10.1016/S0009-2541(97)00145-9 (1998).
45. Santana-Casiano, J. M. *et al.* Significant discharge of CO2 from hydrothermalism associated with the submarine volcano of El Hierro Island. Scientific Reports 6, 25686, doi:10.1038/srep25686

https://www.nature.com/articles/srep25686#supplementary-information (2016).

46. Aya, I., Yamane, K. & Nariai, H. Solubility of CO2 and density of CO2 hydrate at 30 MPa. Energy 22, 263–271, doi:https://doi.org/10.1016/S0360-5442(96)00093-X (1997).
47. Zhao, G. *et al.* Effects of hydrate cap on leakage prevention and capacity improvement of sub-seabed CO2 sequestration. Chemical Engineering Journal 450, 138493, doi:https://doi.org/10.1016/j.cej.2022.138493 (2022).
48. Fahed Qureshi, M. *et al.* Laboratory demonstration of the stability of CO2 hydrates in deep-oceanic sediments. Chemical Engineering Journal 432, 134290, doi:https://doi.org/10.1016/j.cej.2021.134290 (2022).
49. Teng, Y. & Zhang, D. Long-term viability of carbon sequestration in deep-sea sediments. Science Advances 4, eaao6588, doi:10.1126/sciadv.aao6588.
50. Brewer, P. G., Friederich, G., Peltzer, E. T. & Orr, F. M. Direct Experiments on the Ocean Disposal of Fossil Fuel CO2. Science 284, 943–945, doi:10.1126/science.284.5416.943 (1999).
51. Rinnert, E. *et al.* (2019).
52. Cathalot, C., Rinnert, E. & Feuillet, N. (R/V Pourquoi Pas?, 2021).
53. Scalabrin, C. Site d'émissions de fluides, Mayotte, zone Fer à Cheval (C. Scalabrin, 2022). (Ifremer GEO-OCEAN, 2023).
54. Donval, J. P. & Guyader, V. Analysis of hydrogen and methane in seawater by "Headspace" method: Determination at trace level with an automatic headspace sampler. Talanta 162, 408–414, doi:http://dx.doi.org/10.1016/j.talanta.2016.10.034 (2017).
55. Charlou, J.-L. & Donval, J.-P. Hydrothermal methane venting between 12°N and 26°N along the Mid-Atlantic Ridge. Journal of Geophysical Research: Solid Earth 98, 9625–9642, doi:10.1029/92JB02047 (1993).
56. Dumoulin, J. P. *et al.* Status Report on Sample Preparation Protocols Developed at the LMC14 Laboratory, Saclay, France: From Sample Collection to 14C AMS Measurement. Radiocarbon 59, 713–726, doi:10.1017/RDC.2016.116 (2017).
57. Moreau, C. *et al.* ARTEMIS, THE 14C AMS FACILITY OF THE LMC14 NATIONAL LABORATORY: A STATUS REPORT ON QUALITY CONTROL AND MICROSAMPLE PROCEDURES. Radiocarbon 62, 1755–1770, doi:10.1017/RDC.2020.73 (2020).
58. Péron, O., Rinnert, E., Colas, F., Lehaitre, M. & Compère, C. First Steps of in situ Surface-Enhanced Raman Scattering during Shipboard Experiments. Applied Spectroscopy 64, 1086–1093, doi:10.1366/000370210792973505 (2010).
59. Ruffine, L. *et al.* Multidisciplinary investigation on cold seeps with vigorous gas emissions in the Sea of Marmara (MarsiteCruise): Strategy for site detection and sampling and first scientific outcome. Deep Sea Research Part II: Topical Studies in Oceanography 153, 36–47, doi:https://doi.org/10.1016/j.dsr2.2018.03.006 (2018).

Figures

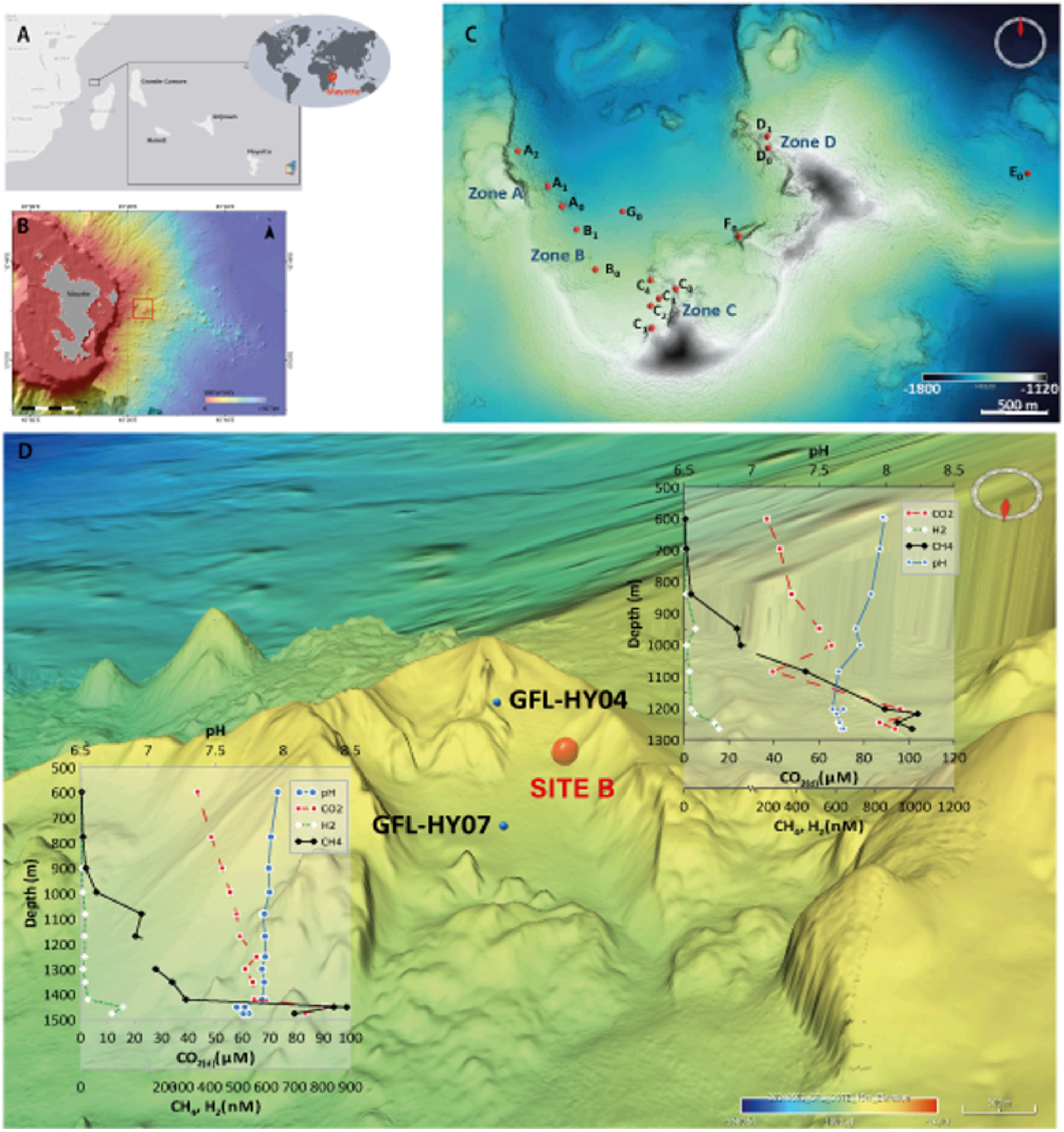

Figure 1

Location of the Horseshoe Area. A. Comoros Archipelago. B. Map of Mayotte Island, the red square indicating the location of the Horseshoe area. C. Active seeping sites location in the Horseshoe area. D. Water column profiles of pH, CO_2, CH_4 and H_2 obtained by CTD/rosette cast and active site B location in the Horseshoe area

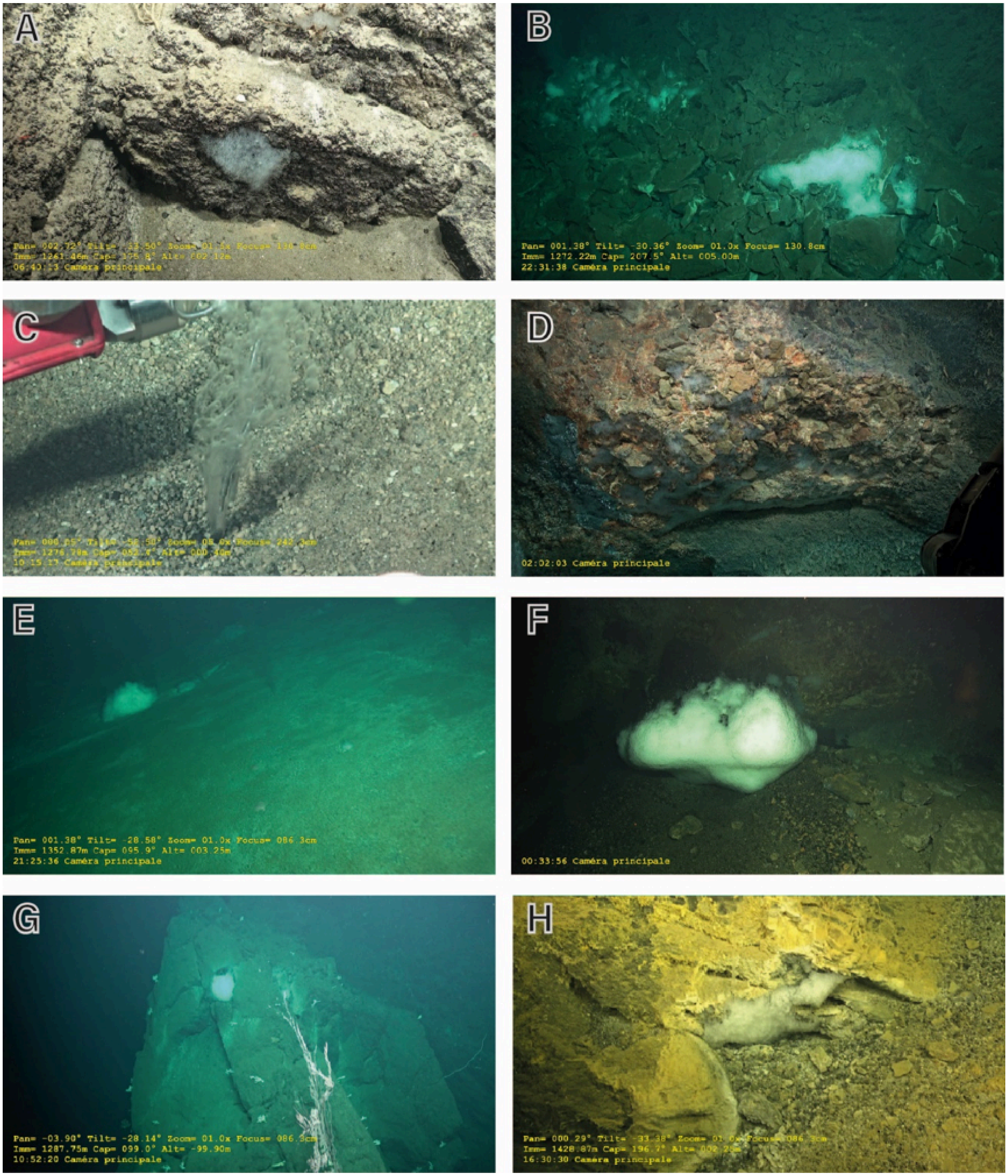

Figure 2

Liquid CO_2 venting in the Horseshoe area. A. CO_2 hydrate under a flange (zone D). B. Hydrates filling up interstices between rocky seafloor at zone C. C. Vigorous liquid CO_2 fountain at site B0. D. Hydrates in crevices from a breccia outcrop (zone C). E. Hydrates mounds and liquid CO_2 fountains seeping through very fine volcanic sand at site B0. F. Massive hydrate mound lying on volcanic sand surrounded by rubble and breccia located 400m SW from zone C. G. Hydrates inserted into crevices at the summit of a phonolite python located at site F0. H. CO_2 hydrates on breccia and rubble covered with filamentous bacteria mats (zone A)

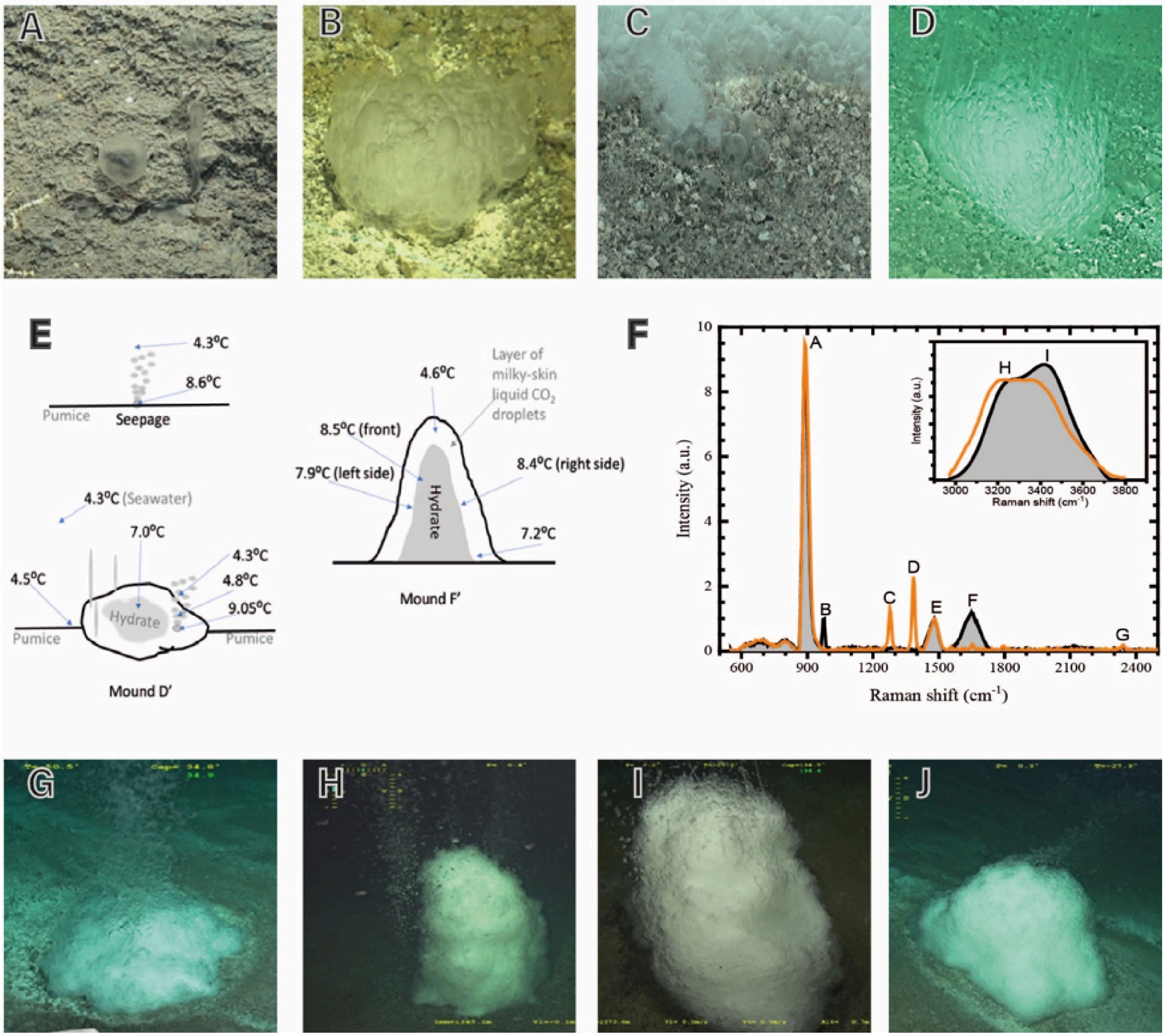

Figure 3

Variability of CO_2 hydrates observed in the Horseshoe area. A: slender droplets formation. B. droplets covered with a hydrate film C. CO_2-rich liquid droplets seeping from a hole surrounded by hydrates (Mound A in Site B). D. CO_2-rich liquid droplets seeping around a small hydrate (Mound D' in Site B0). E. Types of liquid CO_2 fountain, CO_2 hydrates and association observed in the Horseshoe area and temperature gradient at stake. F. *In situ* Raman spectra obtained on hydrate mound F' in site B0 (▯) and surrounding seawater (▯).Vibrational bands assignment: (A, E and G) internal standard, (B) SO_4^{2-} S-O stretching, (C and D) CO_2 Fermi resonance, (F) liquid water OH bending mode, (H) OH stretching modes in hydrate cages and (I) liquid water OH antisymmetric and symmetric stretching modes. G, H, I and J: massive hydrates mounds with liquid CO_2 seeping

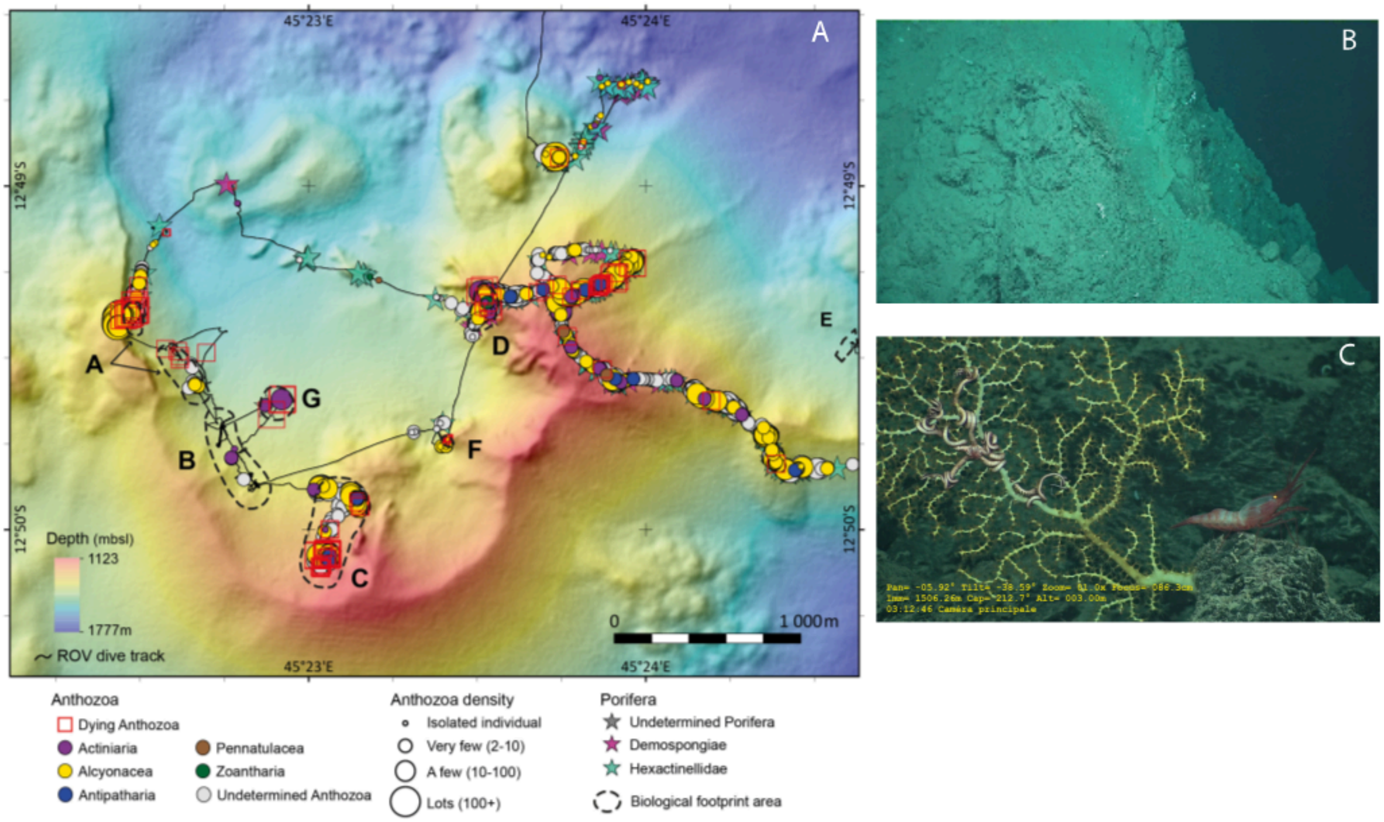

Figure 4

Sessile megafauna in the horseshoe area. A. Distribution of cnidarians and sponges in the horseshoe. B. Example of dead Anthozoa in the proximity of site B0 covered by microbial mats. C. Yellow gorgonian-like Anthozoa.

Supplementary Files

This is a list of supplementary files associated with this preprint. Click to download.

- SupplementaryinfoTable1.xlsx
- ExtendedData.docx
- ExtendedDataFig1.png
- ExtendedDataFig2.pdf
- ExtendedDataFig3.pdf
- ExtendedDataFig4.pdf
- SupplementaryinfovideoEh.wmv

- SupplementaryinfovideositeB.mp4